

## Fractal nature of fat crystal networks

Suresh S. Narine and Alejandro G. Marangoni

*Department of Food Science, University of Guelph, Guelph, Ontario, Canada N1G 2W1*

(Received 23 July 1998; revised manuscript received 15 September 1998)

The quantification of microstructure in fat crystal networks is studied using the relationship of the shear elastic modulus ( $G'$ ) to the volume fraction of solid fat ( $\Phi$ ) via the mass fractal dimension ( $D$ ) of the network. Results from application of a scaling theory (weak-link regime theory), developed for colloidal gels, to the microstructure of fat crystal networks are presented and discussed. A method to measure mass fractal dimensions and chemical length exponents or backbone fractal dimensions ( $x$ ) from *in situ* polarized light microscope (PLM) images of the microstructural network of fat crystals is developed and applied to the fat systems studied. Fractal dimensions measured from *in situ* PLM images of the various fat systems are in good agreement with fractal dimensions measured using rheological measurements and the weak-link regime theory (percent deviations range from 0.40% to 2.50%). The crystallization behavior of the various fat systems is studied using differential scanning calorimetry, and the potential for altering  $G'$  by changing crystallization conditions using the fractal dimension of the network as an indicator is discussed. [S1063-651X(99)00502-4]

PACS number(s): 61.43.-j, 61.41.+e

### I. INTRODUCTION

Some of the most important quality characteristics of fat-containing food products depend on the macroscopic properties of the fat crystal network formed within the finished product. Some of these characteristics include the spreadability of margarine, butter, and spreads, as well as the snap of chocolate. Predicting the macroscopic properties of fat crystal networks within these products is therefore important.

It has been previously established that the hardness of a fat, as determined by large-scale rheological analyses such as cone penetrometry, is directly correlated to the hardness determined by sensory analysis [1–4] (in cone penetrometry measurements, strain levels are of the order of 10%, hence the large-scale classification). Furthermore, measurements in our laboratory indicate that there exists a direct relationship between the elastic modulus (storage shear modulus) of a fat and its hardness index, as determined by cone penetrometry measurements (measurement of shear storage modulus is a small-scale rheological measurement with strain levels of the order of 0.5%). Therefore, the elastic modulus of a fat crystal network is an indicator of the macroscopic consistency of that network.

This paper describes an attempt to utilize scaling theory to derive a theoretical link between the elastic constant of fat crystal networks and the structure of the network, using the fractal dimension of the network as a mathematical indicator of the structure. Many attempts have been made to relate the macroscopic properties of fat crystal networks to the lipid composition (triglycerides) and the polymorphic nature of the network, but these have not been successful. In this paper, we approach the problem from a microstructural perspective. The level of structure of a fat crystal network which most influences its macroscopic behavior is its microstructure, since it is this level of structure which is closest to the macroscopic world. The individual microstructures in fat crystal networks can vary from a diameter of 80  $\mu\text{m}$  to above 120  $\mu\text{m}$ , depending on the system (microstructures in cocoa

butter are shown in Fig. 1), and are therefore closer to the macroscopic level than the structure of the triglyceride molecules or the crystalline units of particular polymorphs. No level of structural “building blocks” larger than the microstructural level has been observed in fat crystal networks, although much evidence of the existence of “clusters” or microstructures of the order of 100  $\mu\text{m}$  have been published, initially by a group at Unilever Research Laboratory in The Netherlands [5–7]. In order to develop our theory, it is first necessary to introduce the various levels of structure of

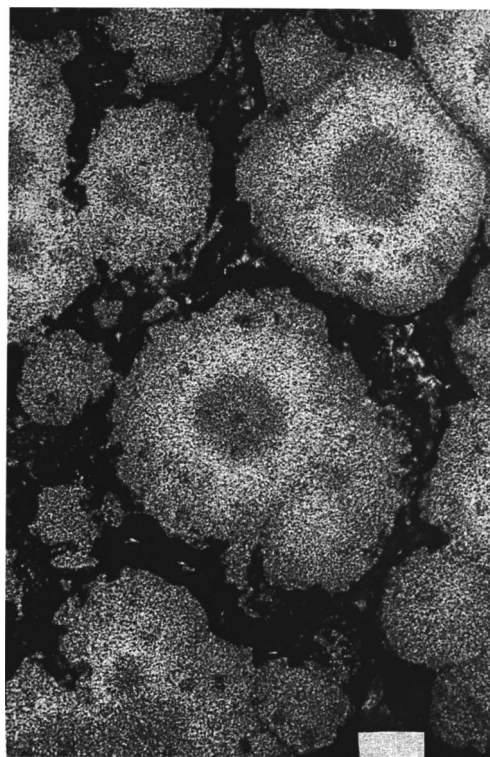


FIG. 1. Gray-scale image of cocoa butter showing the existence of microstructures.

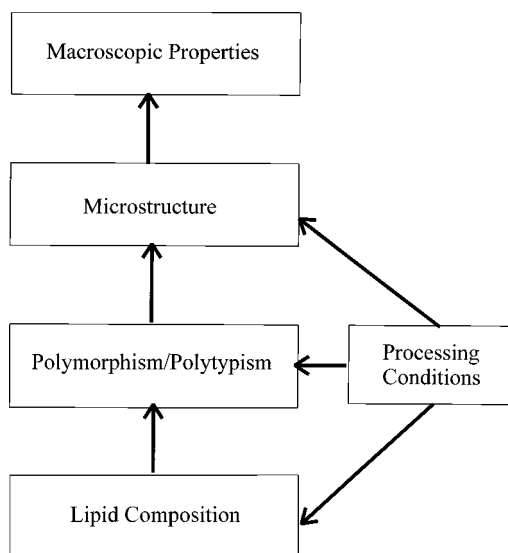


FIG. 2. Schematic of factors influencing the macroscopic properties of a fat crystal network.

a fat crystal network. The flow diagram depicted in Fig. 2 represents our perspective of the various levels of structure and the manner in which they affect the macroscopic properties of the network.

An early mechanical model of fat networks was developed by van den Tempel [8], and extended by various other researchers (reviewed in deMan and Beers) [9], which visualized the fat network as analogous to an assembly of chains, each chain consisting of a linear array of particles packed closely together. The particles making up the chains would interact with each other via van der Waal's forces. Attempts at making this model predictive were not very successful, partly because of the varied nature of the triglycerides present in a typical natural fat crystal network. The calculation of the forces involved between the particles is nontrivial. Additionally, the van den Tempel model suggested that the shear elastic modulus of a particular fat crystal network depends on the solid volume fraction of the network in a linear manner, which has been shown to be untrue by various researchers [10–13].

The growth of a fat crystal network can be visualized thusly: the triglycerides present in the sample crystallize from the melt into particular polymorphic-polytypic states. These crystals then aggregate via a mass- and heat-transfer-limited process into larger microstructures. The aggregation process continues until a continuous three-dimensional network is formed by the collection of microstructures. At the microstructural level, the solid network is an orthodox amorphous solid, while the intramicrostructural level is fractal in nature. In this way, the formation of the fat crystal network is mathematically very similar to a flocculating colloid, the similarity having been noted as early as 1989 by Edwards and Oakeshott [14]. The macroscopic rheological properties of the network are influenced by all levels of structure defined during the formation of the network—i.e., the structure of the individual triglycerides, the structure of the individual crystalline units formed, or the polymorphic nature of the network, and particularly by the microstructural level. Although the microstructural level of the structure is extremely

important to the scaling behavior of the network, and therefore to the elastic properties, lipid composition and the polymorphic-polytypic nature of the network also play a major role. The microstructural level is important to the scaling behavior of the network because the microstructures are composed of elements that are arranged in a fractal geometry within each microstructure. Therefore, in any consideration of factors influencing the macroscopic properties of the fat crystal network, there is a need to consider the microstructural effects. As can be appreciated, because of the complex, random, nature of the aggregated structures, an extension of the van den Tempel model to this perspective of the fat crystal network is not simple, although some attempts have been made [15–17].

An exciting period in the analysis of polymer and colloidal networks ensued after the introduction of the fractal concept in 1982 [18]. Since then, scaling theory has been used to explain the elastic properties of polymer gels [19–22]. Much progress was made in the analysis of the microstructure of colloidal aggregates, the verdict being that they are fractal structures, which are quantifiable from rheological and optical measurements [23–31]. Early development of a scaling theory to explain the elastic properties of colloidal gels were performed by Brown and Ball [24,26,29]. Brown and Ball suggested that colloidal aggregates should behave as stochastic mass fractals on a scale which is large compared to the primary particle size, and formulated a power-law relationship of the elastic modulus to the solid volume fraction. This formulation was experimentally verified by various others, including Sonntag and Russel [27] and Buscall *et al.* [28]. In 1990, Shih *et al.* [30] outlined the development of a scaling theory to explain the elastic properties of colloidal gels by again considering the structure of a colloidal network as a collection of fractal flocs, except that their paper defined two separate regimes depending on the concentration of the colloidal gel. At low concentrations, the strong-link regime was appropriate, the formulation of which is identical to the formulation of Brown [26]. At high concentrations, the weak-link regime is appropriate, which differs in formulation from the strong link regime and that suggested by Brown and Ball [24,26,29].

In 1992, Vreeker *et al.* [13] presented an interpretation of rheological data for aggregated fat networks in the framework of fractal theories. These authors showed that the elastic modulus ( $G'$ ) varied with particle concentration ( $\Phi$ ) according to a power law, in keeping with the models for the elasticity of colloidal gels proposed in Refs. [24,26,29,30]. Recently, Marangoni and Rousseau [32] applied Shih *et al.*'s weak-link formulation concept to high  $\Phi$  systems, from a rheological perspective. Using the argument of similar particle-aggregation type systems, our view of fat microstructural networks as a mass- and heat-transfer-limited particle aggregation process lends itself well to the type of scaling behavior analysis exploited in the treatment of colloidal gels. In our picture of the fat crystal network the average floc size in a colloidal network is replaced by the average size of the microstructures. As Shih *et al.* [30] considered the flocs in a colloidal gel as fractal objects, so do we consider the collection of microstructural elements in a microstructure to be fractal in terms of the distribution of mass. The microstructural elements pack in a manner peculiar to the particu-

TABLE I. Summary of fat networks studied rheologically with corresponding fractal dimensions and values of  $\gamma$ .

Fat system	Fractal dimension $D$	Pre-exponential factor $\gamma$ (MPa)
NIE milkfat 1	2.45	$1.0 \times 10^{-3}$
CIE milkfat 1	2.16	$9.5 \times 10^{-3}$
NIE milkfat 2	2.59	$4.6 \times 10^{-4}$
EIE milkfat 2	2.50	$9.9 \times 10^{-4}$
NIE milkfat 3	1.96	$2.6 \times 10^{-1}$
(DMA analysis)		
NIE milkfat 4	2.01	$2.2 \times 10^{-1}$
(DMA analysis)		
NIE palm oil	2.82	$1.2 \times 10^{-9}$
CIE palm oil	2.82	$2.0 \times 10^{-9}$
NIE lard	2.88	$9.2 \times 10^{-14}$
CIE lard	2.84	$6.7 \times 10^{-10}$
Cocoa butter 1	2.37	$5.3 \times 10^{-2}$
Cocoa butter 2	2.40	$2.1 \times 10^{-2}$
(DMA analysis)		
Salatrim™	2.90	$4.9 \times 10^{-19}$
Tallow	2.41	$1.5 \times 10^{-2}$

lar fat, and the microstructures themselves fill the volume of the sample as statistically repeating units of the fat crystal network.

Interest in the microstructure of fat crystal networks in our laboratory arose during studies of factors affecting the hardness and spreadability of chemically interesterified (CIE) and enzymatically interesterified (EIE) milkfat [32–37]. The hardness of CIE and EIE milkfat at equivalent  $\Phi$  values were lower than their noninteresterified (NIE) counterparts [36–37]. Palm oil, lard, cocoa butter, Salatrim™ [38–41], and tallow were also studied. The weak-link theory of Shih *et al.* was utilized in an attempt to explain these results. The analyses done on these systems were all rheological, but yielded, according to the theory outlined below, fractal dimensions recorded in Table I.

The main focus of this paper is to attempt to verify the scaling theory governing the calculation of fractal dimensions obtained from rheological methods. Polarized light microscopy was used as a method of imaging samples of fat crystal networks at the microstructural level, and the images analyzed to yield fractal dimensions. The fractal dimensions

were then compared to the values determined rheologically for similar fat systems. Very good agreement was found between the fractal dimensions determined rheologically and by image analysis of the networks, as is shown in Table II. Furthermore, analysis of the fat crystal network at the microstructural level has yielded important insights into the nature and influence of various levels of physical structure within a fat crystal network.

The crystallization behavior of the different fat systems was studied using differential scanning calorimetry (DSC). Results from these studies have helped clarify the relationship between fractal dimension and structure. The fact that one can utilize temperature conditioning during crystallization to alter the fractal dimension of the network, and therefore the storage shear modulus, has also been explained via crystallization curves of the fat systems.

## II. THEORY

Fractal systems are self-similar at all levels of magnification, and unlike Euclidean systems, which have integral dimensions ( $d$ ), have fractional dimensions ( $D$ ). We recommend the reviews by Jullien and Botet [42] and Meakin [43] on the subject of fractal aggregation. Aggregates scale in a fractal manner in the range between the size of the individual particles composing the clusters or flocs (microstructures) and the size of the microstructure. For colloidal aggregates (and by extension fat crystal networks), the fractal concept quantifies the way in which the mass  $M$  of the microstructure increases with its radius  $R$ , according to the fractal dimension  $D$  [13,31,42]:

$$M \sim R^D, \quad (1)$$

where the symbol  $\sim$  is taken to mean “approximately proportional to.” It has been shown experimentally that the elastic properties of fat crystal networks are dominated by the fractal nature of the microstructure [13,32–41]. For the elastic shear modulus  $G'$ ,

$$G' \sim \Phi^m, \quad (2)$$

where  $\Phi$  is the particle volume fraction of solid fat and  $m$  depends on the fractal dimension.

Following is a description of a theory submitted by Shih *et al.* [30] on the scaling behavior of the elastic properties of colloidal gels under two regimes. These regimes are depen-

TABLE II. Fractal dimension calculated via image analysis compared to fractal dimension calculated via rheology using the weak link theory of Shih *et al.* [30]. Errors in  $D$  are standard errors of 3 replicates.

Fat system	Fractal dimension from image analysis	Fractal dimension from rheology (weak link regime)	Percent deviation	Backbone fractal dimension $x$
Cocoa butter 1	$2.31 \pm 1.7\%$	$2.37 \pm 4.0\%$	2.5	1.10
NIE milkfat 4 (Analyzed using DMA)	$2.02 \pm 1.2\%$	$2.01 \pm 15.7\%$	1.5	1.00
Palm oil	$2.82 \pm 0.6\%$	$2.82 \pm 0.6\%$	0.0	1.10
Lard	$2.86 \pm 0.6\%$	$2.88 \pm 0.5\%$	1.0	1.15
Tallow	$2.42 \pm 1.2\%$	$2.41 \pm 6.4\%$	0.4	1.10

dent upon the strength of the links between the clusters (microstructures in the fat crystal network) of a colloidal gel relative to the strength of the clusters themselves. Because of the similarities between colloidal gels and fat crystal networks, this theory has been adapted for fat crystal networks.

### A. Strong-link regime

For colloidal gels, at low particle concentrations, the strong-link regime is applicable. In this case, the individual clusters grow large, so that each acts like a weak spring. Therefore, the elastic constant of the system as a function of particle concentration is dominated by the elastic constant of the flocs. We did not consider the elastic constants of the microstructures in our approach, since we assumed that, in fat crystal networks, the links between microstructures are more likely to be stressed when the entire network is stressed, rather than the microstructures themselves. As shown by the results we obtain, it seems that this assumption is correct, since there is good agreement between fractal dimension calculated rheologically and from image analysis of images obtained by microscopy. For the strong-link regime, the following relationship is suggested by Shih *et al.* [30]:

$$G' \sim \Phi^{[(d+x)/(d-D)],} \quad (3)$$

where  $x$  is the backbone fractal dimension (chemical length exponent) or tortuosity of the network: usually a number which is less than the fractal dimension of the network, but larger than unity in order to provide a connected path. Shih *et al.* [30] found that, for the colloidal gels they studied,  $x$  was a value between 1 and 1.3. In this paper we present a method to calculate  $x$ .

### B. Weak-link regime

The weak-link regime behavior is observed at high particle concentrations. Here the intermicrostructural links are weak compared to the intramicrostructural links and therefore the elastic constant of the system is dominated by the elastic constant of the links between the microstructures. The macroscopic elastic constant  $K$  of a system of size  $L$  can be written in terms of the intermicrostructural links,

$$K \sim \left[ \frac{L}{\xi} \right]^{d-2} K_l \sim \xi^{-(d-2)}, \quad (4)$$

where  $K$  is the elastic constant of the system,  $K_l$  is the elastic constant of the intermicrostructural link, and  $\xi$  is the average microstructural size. If the fractal dimension of the microstructures is  $D$ , the scaling relationship between the average microstructural size  $\xi$  and the solid volume fraction  $\Phi$  can be found by approximating the solid volume fraction inside the microstructures as the overall solid volume fraction:

$$\xi \sim \Phi^{1/(D-d)}. \quad (5)$$

This relation is well known in semidilute polymer solutions [19], and was shown by Dietler *et al.* [44] to be correct for colloidal silica gels as well. We make use of the relationship for fat crystal networks because of their above-mentioned similarity to colloidal gels. Combining Eqs. (4) and (5) yields

$$K \sim \Phi^{[(d-2)/(d-D)]} \sim G'. \quad (6)$$

Therefore, from this theoretical basis, for fats with a high volume fraction of solids, the elastic modulus increases as a function of  $\Phi$  in a power-law manner, with slope  $[(d-2)/(d-D)]$ , or  $[1/(d-D)]$  since the samples examined are three dimensional. Depending on the regime, the value of  $m$  in Eq. (2) can be calculated from Eqs. (3) or (6). Bremer, van Vliet, and Walstra [22] noted that Eq. (2) can be written as

$$G' = \gamma \Phi^m, \quad (7)$$

where  $\gamma$  is a constant independent of the volume fraction, but dependent on the size of the primary particles and on the interactions between them. This seems to suggest that the value of  $\gamma$  will depend on the polymorphic nature of the fat crystal network, which in turn will depend on the particular lipid or triglyceride composition of the sample and on the processing conditions used to crystallize the sample from the melt. Significantly different polymorphic states can be achieved from the same sample, depending on processing conditions, as shown in the case of tripalmitin [45]. This therefore makes a strong case for the study of the influence of polymorphism on  $\gamma$ , which is currently underway in our laboratory.

From Eq. (7), the macroscopic elastic constant of a network of particles is a function of both the spatial distribution of aggregating particles, characterized by the fractal dimension, and the mechanical properties of the particles which make up the network. Information on the elastic constant of the particles is contained in the parameter  $\gamma$ . Knowledge of the fractal dimension of the network may be used to infer the mechanism by which the network was formed (diffusion-limited, reaction-limited, cluster-cluster aggregation, etc.) [46–48].

## III. EXPERIMENTS

### A. Relationship between hardness index and elastic modulus

The method used to analyze samples for hardness index was described in Ref. [4]. In brief, the average sensory impression of hardness of NIE, CIE, and EIE milkfat and milkfat–canola oil blends made by 11 panelists was plotted against the  $\log_{10}$  of the penetration depth, measured in units of 0.1 mm, of a cone penetrometer. It was found that sensory hardness is inversely proportional to the penetration depth. The hardness of fats is directly related to their yield value [1], and an instrument which adequately measures the yield value of fats is the cone penetrometer, various types of which are described in the early literature [49–51]. Fats become softer when kneaded or deformed on a large scale, so therefore to reduce these deformations to a minimum, hardness is measured at low-velocity gradients. When a cone is used to penetrate a fat sample, the velocity with which it moves through the fat is small, resulting in low-velocity gradients. The cone is usually made of metal, such as stainless steel or aluminum, and is lowered into the sample for a fixed time. The penetration depth is then measured, usually via a scale that is attached to the cone itself. The scales are usually graduated in 0.1 mm. As shown in Ref. [4], the penetration

to which a cone of constant shape and weight reaches into a particular sample is inversely correlated to the hardness index of the sample. Therefore, the units of hardness index are  $0.1 \text{ mm}^{-1}$ , since those of cone penetrometry measurements are  $0.1 \text{ mm}$ .

Values of storage (elastic) modulus for samples of NIE milkfat, palm oil, and lard; CIE milkfat, palm oil, and lard; and EIE milkfat were calculated according to the rheological methods outlined below. Different  $\Phi$  values were also obtained for each material by using canola oil as a diluent for the milkfat and lard samples, soyabean oil was used as a diluent for the palm oil samples, and  $\Phi$  measured for each. Cone penetrometry measurements were performed on similarly prepared samples as well, and the hardness index calculated from the cone penetrometry measurements as the inverse of the penetration depth. Elastic modulus for each fat system at the different  $\Phi$  values were then plotted as a function of hardness index.

### B. Rheology

The rheological analysis of this theory was performed by plotting  $\ln(G')$  of the macroscopic systems as a function of  $\ln(\Phi)$ . The slope of this plot gives the value of  $m$ , from Eq. (7). Systems studied rheologically in our laboratory were NIE, CIE, and EIE milkfat [32–37]; NIE and CIE palm oil and lard [38–40]; cocoa butter; and Salatrim [41] and tallow. The determination of  $\Phi$  was performed by pulsed nuclear magnetic resonance (NMR) using a Bruker PC/20 series NMR Analyzer (Bruker, Milton, ON, Canada) as outlined in Ref. [32]. The melted fats were placed in NMR tubes, and crystallized in a refrigerator according to different tempering conditions as outlined in Refs. [32–41]; for tallow, from the melt, the fat was allowed to crystallize at  $5^\circ\text{C}$  for 24 h. The storage or shear elastic modulus  $G'$  of the plastic fats was determined as outlined in Ref. [35].

The following is a general description of the sample preparation and method used for the rheological measurements. Any minor deviations from this method when performing the measurements on the various fat systems studied [32–41] are noted in the corresponding Refs. [32–41], and the measurements for tallow were performed exactly as described here. All rheological measurements were made using a CarriMed CSL<sup>2</sup> 500 Rheometer (TA Instruments) with a 2-cm parallel plate attachment. One of the attachment plates is a Peltier plate, which allows the samples to be analyzed at specific temperatures ( $5^\circ\text{C}$  for all samples excepting Salatrim<sup>TM</sup> and cocoa butter, which were analyzed at  $20^\circ\text{C}$ ). The liquefied blends of the fat were poured into molds in order to ensure uniform diameters and thickness for the samples. The diameter of the resulting samples is the same as the diameter of the attachment plates on the CarriMed machine. The thickness of the sample is an important parameter, since too thick a sample makes it impossible to attain a uniform strain field through the sample, while too thin a sample results in interference due to particulates. We have used a sample thickness of 3.2 mm. The fats were allowed to crystallize in the molds according to the different tempering conditions listed in the above-mentioned references [32–41]. To prevent slippage between the sample surface and the surface of the sample-attachment of the CarriMed, 50 grit sandpaper

was attached to both the sample attachment plate and the surface of the Peltier plate, with Krazy Glue<sup>TM</sup>. The sample was then compressed to approximately 10% of its original thickness, utilizing the software interface of the CarriMed, the compression force being applied in an exponentially increasing manner at a rate of  $50 \mu\text{m/s}$ . The reason for this compression was to ensure that the sandpaper was thoroughly embedded into the sample, thereby preventing surface slippage. Except for cocoa butter, with which just Krazy Glue<sup>TM</sup> was used, sandpaper was used with all of the fat systems studied to ensure no slippage.

After the sample was mounted in the manner described above, the rheometer was run through an oscillatory stress program, with applied stresses ranging from 1 to 31 800 Pa at a frequency of 1 Hz. This stress program was performed in order to determine the boundaries of the linear viscoelastic region (LVR). One has to exercise caution in the determination of the LVR since it is absolutely imperative that the machine is being operated at strain levels that are above its minimum detection limit. For the CarriMed CSL<sup>2</sup> 500, a strain of approximately 0.02% is the minimum detection limit. On establishing the LVR, frequency sweeps of the material can be carried out by applying either a constant stress or a constant strain. Generally, frequency sweeps were carried out over a frequency range of 0.1–10 Hz at a strain level of 0.2–0.5%. Apparent storage and loss moduli ( $G'$  and  $G''$ ) values were obtained from both the stress sweeps and the frequency data.

Additionally, milkfat–canola oil mixtures and cocoa butter–canola oil mixtures were analyzed using dynamic mechanical analysis. The sample preparation method was different from that used with the CarriMed. Milkfat–canola oil mixtures and cocoa butter–canola oil mixtures (100%, 90%, 85%, 80%, 75%, and 70% w/w) were melted above  $60^\circ\text{C}$  for 30 minutes and poured into 1-cm-diameter plastic syringes. The milkfat–canola oil samples were then placed in a refrigerator and crystallized statically for 24 h at  $5^\circ\text{C}$ , and the cocoa butter–canola oil samples were allowed to crystallize at  $5^\circ\text{C}$  for 1 h and then at  $20^\circ\text{C}$  for 24 h.

Dynamic mechanical analysis was performed with a Perkin Elmer DMA 7 machine using parallel-plate geometry (1-cm-diameter circular plate). Milkfat and milkfat–canola oil disks and cocoa butter and cocoa butter–canola oil disks were prepared by pushing the crystallized samples out of the syringe using the syringe plunger, and cutting 0.5-cm-thickness disks. These disks were then quickly transferred into the  $5$  and  $20^\circ\text{C}$  temperature-controlled DMA cell. The upper plate was lowered manually until contact with the sample was established. All compression measurements were performed under a static force of 5 kPa to ensure proper mechanical contact. On top of the static stress, a dynamic stress wave was applied at a frequency of 1 Hz, increasing from 2.5 to 5 kPa at 1 kPa/min. A clear linear viscoelastic region was observed in this stress range, and compressive storage ( $\varepsilon'$ ) and loss ( $\varepsilon''$ ) moduli were derived. Strains were in the range of 0.01%. Since  $\varepsilon'$  is related very closely to  $G'$ , we took measurements of  $\varepsilon'$  as independent checks of  $G'$ .

No irreversible structural changes seemed to have been introduced by the strains applied to the fat samples, either during analysis by the DMA or by the CarriMed. This was established by doing repetitions of measurements; it was no-

ticed that the measured values of  $G'$  and  $\varepsilon'$  remained the same after previous measurements. Working in the LVR ensures that there is no irreversible structural changes to the network.

The  $\ln$  of the obtained values of  $G'$  and  $\Phi$  were plotted against each other, and the slope of the line,  $m$ , was determined by linear regression. Assuming a weak-link regime, the slope of this line is related to the fractal dimension via Eq. (6).

### C. Polarized light microscopy

Samples of milkfat-canola, cocoa butter-canola, Salatrim<sup>TM</sup>-canola, palm oil-soya bean oil, lard-canola, and tallow-canola blends were analyzed using polarized light microscopy images of the intramicrostructural network of the particular fat crystals. As early as the 1960s, polarized light microscopes were used to analyze the birefringent solid structures of fat crystal networks [52]. Lately, birefringent properties of solid fat crystals have been used as a means of diagnosis in the medical field [53].

The samples were prepared by melting the prepared blends of the fat systems at 80 °C, and using a Pasteur pipette to deposit a small droplet of fat onto a glass slide preheated to the temperature of the melted fat. A similarly heated glass coverslip was then dropped onto the surface of the droplet, ensuring that the plane of the coverslip was parallel to the plane of the slide. This allowed the droplet to be smeared out into an extremely thin rectangular block of fat of uniform thickness. The samples were then allowed to crystallize in a refrigerator and/or at room temperature, care being taken to follow the tempering procedure used for the particular fat system during preparation of the sample for rheology. A polarized light microscope (PLM) was then used to investigate the structure of the microstructural networks of the fat systems *in situ*.

PLM images of milkfat-canola, palm-soya bean oil, lard-canola, and tallow-canola blends were photographed at 5 °C after being in the refrigerator at 5 °C for 24, 72, 24, and 24 h, respectively. Cocoa butter-canola and Salatrim<sup>TM</sup>-canola mixtures were photographed at room temperature after being refrigerated at 5 °C for 1 h and then allowed to sit at room temperature for 24 h.

### D. Image analysis

The photographs made of the images of the fat systems under the PLM were scanned into a Pentium 200-MHz IBM-compatible computer using a Hewlett-Packard 6100C scanner. In order to analyze the photographs of the polarized micrographs taken of the fat systems, the images were thresholded. In order to do this, a particular threshold value has to be utilized, which allows all of the microstructural elements to be seen as white, and all of the background to be reduced to black. This is an especially difficult and crucial task, since one has to take care to ensure that all of the solid particles are represented in the resulting thresholded image. Algorithms exist to calculate threshold values; one such method that was used in this study is the statistical correlation method [54].

The statistical correlation method was used to calculate threshold values for some of the images scanned into the

computer, but since each time we were able to judge the threshold value by eye within one or two points, human judgment of the threshold value was used in most of our analysis. In some cases, this involved causing microstructural elements in focus to appear slightly larger than they were under the magnification used, in order to ensure that the microstructural elements out of focus were counted as particles. In this way, it became obvious that any fractal analysis of the images was going to have to be performed by counting particles, since one could not perform a spatial dimension measurement such as measurement of the Hausdorff Dimension [55–58]. It was important to ensure that all the microstructural elements were represented, for essentially we were projecting all of the microstructural elements onto the plane of focus of the image, so that the resulting fractal dimension calculated would have been in a system with  $d=3$ . When the image was thresholded, the out-of-focus (due to the depth of the sample) particles were represented in the focal plane of the image, and therefore could be counted as contributing to the mass of the system. When calculating the mass fractal dimension of a system, as will be explained below, the number of particles in a cube of a length  $R$  through the sample is counted. Therefore, by “projecting” the out-of-focus microstructural elements into the plane of the image so that they could be counted, one can count the number of particles that is present in the sample in a cube the length of which is equivalent to the length of a square drawn in the plane of the image.

## E. Fractal dimension

### 1. Traditional methods

The method that was used in our determination of fractal dimension from the PLM images differed somewhat from traditional methods. There are several different concepts of the fractal dimension of a geometrical configuration. The most famous method of calculating fractal dimensions in the natural sciences in the so-called box counting dimension. Many excellent volumes have been written on the subject, and for a description of the traditional methods, we recommend the books by Falconer [55], Crowover [56], and Mandelbrot [18].

### 2. Particle-counting method

The images of the fat networks that were acquired from our PLM were not suitable for analysis by the traditional methods of fractal dimension determination. The reason for this is because our images were subsets of two-dimensional space, but represented a subset of a three-dimensional network. Furthermore, because of the need to utilize thresholding methods to ensure the representation of all the microstructural elements within the two-dimensional image, the size of the microstructural elements already in focus was increased, while those out of focus appeared smaller than the magnification warranted. Therefore, the size of the individual microstructural elements were not representative of the size of the fractal, at whatever magnification the picture was taken.

If we assume that the constituent particles (microstructural elements) of a particular microstructure were of the same average diameter (not a bad assumption, from examin-

ing Figs. 5–7), then for calculation of the mass fractal dimension, it is sufficient to just count the particles, regardless of whether some appear larger when the image is thresholded. Therefore, we count the number of particles present in a three-dimensional portion of the sample by first representing all of the particles present in that portion of the sample in the plane of the image. Of course, we miss those particles that did not appear in the picture due to geometrical shadowing, but the number of these can be rendered negligible by making the thickness of the sample very small. Since we were essentially restricted by the nature of our representation of the fractal (fat crystal network) to counting microstructural elements, we utilized Eq. (1). This equation stems from one of the principal characteristics of a particle-aggregation fractal system, where the fractal dimension  $D$  relates the number of particles  $N$  to the linear size of the fractal  $R$  and the linear size of one particle (microstructural element)  $\sigma$ :

$$N = \left(\frac{R}{\sigma}\right)^D, \quad N \gg 1. \quad (8)$$

Here, the fractal object is a mass fractal (a microstructure), and  $\sigma$  refers to the radius of the particles constituting the fractal, while  $R$  corresponds to the radius of the entire fractal object. One can approximate  $R$  to be the length of a cube that just covers the entire fractal object if the fractal is in a  $d = 3$  system, the length of a square for a  $d = 2$  system and length of a line for a  $d = 1$  system. Assuming a statistically constant particle size, or in our case, a statistically constant microstructural element size,

$$N \propto R^D. \quad (9)$$

Taking logarithms,

$$\log_{10} N(R) = \log_{10} c + D \log_{10} R, \quad (10)$$

where  $c$  is a constant greater than 1,  $N(R)$  is the number of particles in the fractal of length  $R$ , and  $R$  is the length of the line segment, the length of a side of a square, or the length of a side of a cube which covers or envelopes the fractal. The lower limit of this relationship then becomes the size of one microstructural element, i.e.,  $R = a$ , and  $N(R) = 1$  is the lower limit. Therefore, proceeding in like manner to the traditional form of box counting,  $N(R)$  for various values of  $R \gg a$  is counted, and  $\log_{10}(N(R))$  plotted vs  $\log_{10}(R)$ , the resulting slope of the line being equal to  $D$ . Since  $N(R)$  determined this way is only an approximation, more points in such a plot serves to decrease the error.

(a) *Fractal dimension  $D$* . In order to calculate the value of  $D$  (with  $d = 3$ ), we count the number of microstructural elements  $N(R)$  projected onto a square area of the side of length  $R$ , drawn in the focal plane of the image. This count represents the number of particles present in a cube of length  $R$  through the fractal. Figure 3(a) shows a schematic of the projection of microstructural elements onto the area of side  $R$ . Values of  $\log_{10}(N(R))$  were plotted against  $\log_{10}(R)$  for varying values of  $R$ . The resulting slope of the line was taken as being equal to  $D$ .

(b) *Fractal backbone dimension  $x$* . The fractal backbone dimension of the network may be thought of as an indicator of the spatial distribution of the microstructural elements in

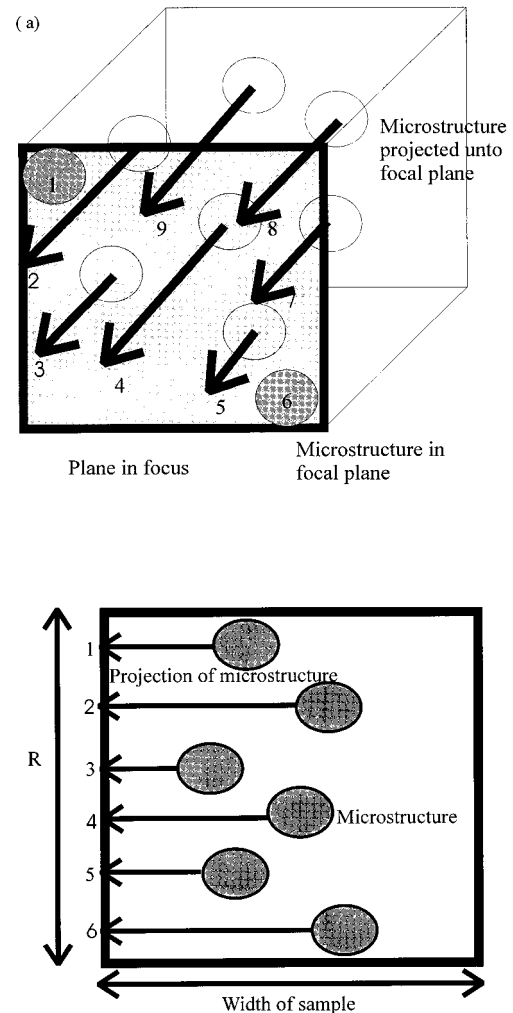


FIG. 3. Schematic of a sample showing how the fractal dimension ( $D$ ) and tortuosity ( $x$ ) are calculated.

chains of these elements constituting a microstructure. It is understood that these “chains” are arbitrary in terms of which microstructural elements belong to which chains. These chains are of course in a  $d = 2$  space, and therefore a variation of Eq. (8) in a two-dimensional system is applicable,

$$N \sim \left(\frac{R}{\sigma}\right)^x, \quad (11)$$

where  $R$  is the length of an area enveloping the fractal chain, and  $x$  is the backbone fractal dimension, chemical length exponent, or tortuosity. The thresholded images of our fat crystal networks represent all the particles in the  $d = 3$  network projected onto the plane of the image. Therefore, a vertical straight line drawn on the thresholded image will intersect all of the particles that belong to a particular chain that lies in the plane perpendicular to the plane of the image and which intersects the vertical line. Figure 3(b) represents a cross-sectional view of the sample, showing the projection of the various microstructural elements onto the plane of the photograph or image. Therefore, by measuring various lengths of the vertical line, one is in effect measuring various lengths of the area that envelops particles in the plane that

intersects the vertical line, and is perpendicular to the plane of the image. Therefore, to calculate  $x$ , we counted the number of particles  $N(R)$  that intersects a vertical line drawn in the plane of the image for different values of  $R$ . A plot of  $\log_{10}(N(R))$  against  $\log_{10}(R)$  then yields  $x$  as its slope.

#### F. Crystallization behavior

Samples of milkfat, cocoa butter, palm oil, lard, and tallow were melted to above  $60^\circ\text{C}$  and immediately placed inside sealed aluminium pans. A Dupont Model 2090 differential scanning calorimeter was used to monitor changes in heat flow during crystallization of the samples. Similar, empty pans were used as standards. The machine was operated at a rate of  $5^\circ\text{C}$  per minute. Samples of tallow, cocoa butter, and palm oil were cooled at this rate down to  $-20^\circ\text{C}$ , while lard was cooled down to  $-30^\circ\text{C}$  and milkfat to  $-40^\circ\text{C}$ .

#### IV. RESULTS

A proportional relationship was seen to exist between elastic modulus and hardness index for each of the samples studied, the  $r^2$  values of the resulting straight lines of plots of  $G'$  vs hardness index ranging from 0.87 to 0.99. An example of a plot of elastic modulus vs hardness index is shown in Fig. 4(a) (in this case, the plot is for NIE lard–canola oil mixtures).

A typical graph of  $\ln G'$  vs  $\ln \Phi$  (or  $\ln \varepsilon'$  vs  $\ln \Phi$  for DMA analysis) for samples analyzed using the CarriMed rheometer is shown in Fig. 4(b) (this graph was for tallow) and for cocoa butter–canola oil samples analyzed using the DMA is shown in Fig. 4(c). Figure 4(b) supports the power law relationship  $G' = \gamma\Phi^m$ ; the resulting straight lines of plots of  $\ln G'$  vs  $\ln \Phi$  for all the fat systems studied are characterized by high  $r^2$  values. As is demonstrated by Fig. 4(c), rheological analysis by the DMA is equally as supportive of the  $G' = \gamma\Phi^m$  relationship. Additionally, analysis of this type allows a value to be calculated for the pre-exponential term  $\gamma$ . Values of  $\gamma$  are recorded in Table I, together with values of fractal dimension  $D$  calculated using the weak link theory of Shih *et al.* [30] for the various fat systems that have been studied rheologically.

Figures 5(a), 5(c), 6(a), 6(c), 7(a), and 7(c) show gray-scale photographs of lard, palm, cocoa butter, milkfat, tallow, and Salatrim™, respectively. The entire solid mass of the thin samples is represented in the pictures, although some of the microstructural elements are out of focus due to the depth of the samples. The thresholded images for all the systems studied are shown in Figs. 5(b), 5(d), 6(b), 6(d), 7(b), and 7(d).

Fractal dimensions calculated for the various fat systems studied are summarized in Table II. For each particular fat system, three samples of different values of  $\Phi$  were analyzed, and the average of the resulting fractal dimension reported in Table II, together with the standard error. An example of a plot of  $\log_{10}(N(R))$  vs  $\log_{10}(R)$  is shown in Fig. 8(a) (for an 85% w/w blend of milkfat and canola oil).

Values of  $x$  calculated for the various fat systems studied are summarized in Table II. An example of a plot of  $\log(N(R))$  vs  $\log(R)$  to calculate  $x$  is shown in Fig. 8(b) (for an 85% w/w blend of milkfat and canola oil). Figure 9 shows

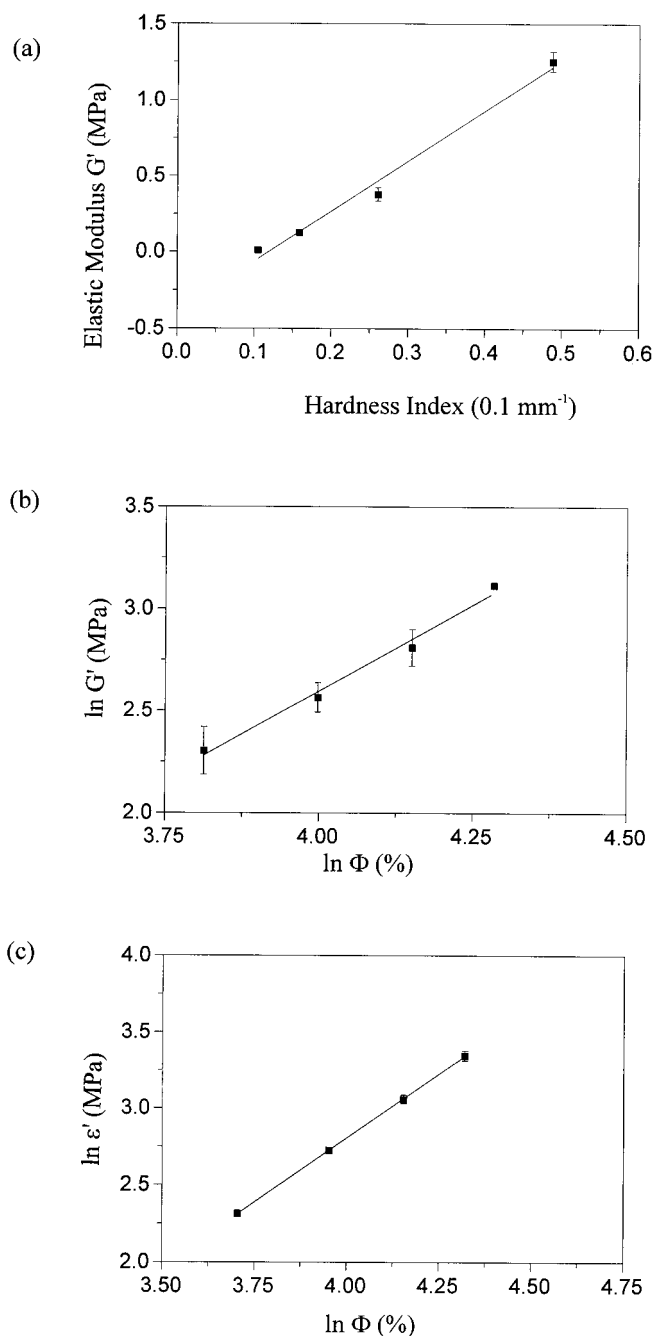


FIG. 4. (a)  $G'$  as a function of hardness index for a sample of lard. (b)  $\ln(G')$  as a function of  $\ln(\Phi)$  for a sample of tallow. (c)  $\ln(\varepsilon')$  as a function of  $\ln(\Phi)$  for cocoa butter. The solid lines in all the graphs represent the best fit line through the points, calculated by linear regression.

plots of heat flow vs temperature for lard, palm, cocoa butter, milkfat, and tallow.

While the rheological analysis worked well with the samples studied, it is unsuitable for softer fats. In addition, rheological analysis leading to the calculation of a fractal dimension does not provide any insight into the parameters that affect the value of  $D$ , since it is based on macroscopic measurements. However, the fact that a fractal dimension, which is distinctly different for different fat networks, can be calculated using this method allows one to analyze the effect of fractal dimension changes on elastic constants of the fat

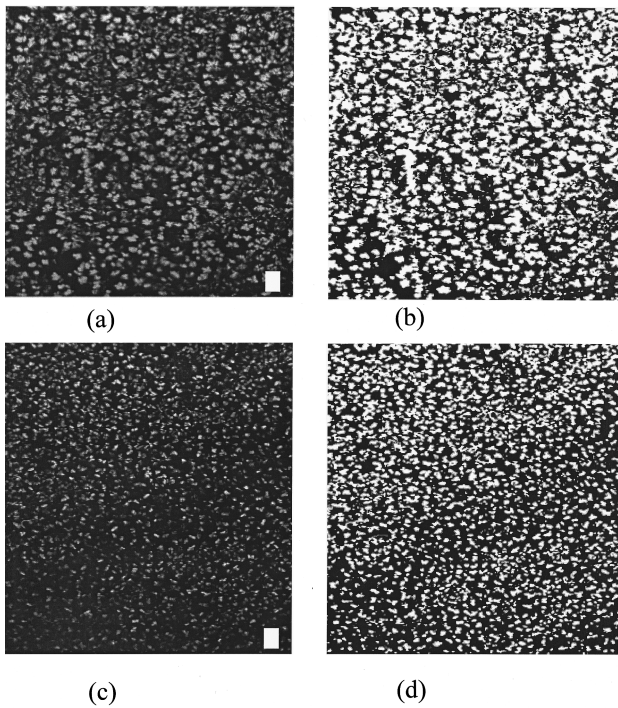


FIG. 5. (a) Gray-scale image of a sample of lard. (b) Thresholded image of (a). (c) Gray-scale image of a sample of palm oil. (d) Thresholded image of (c). The horizontal length of the inset bar represents 0.005 mm.

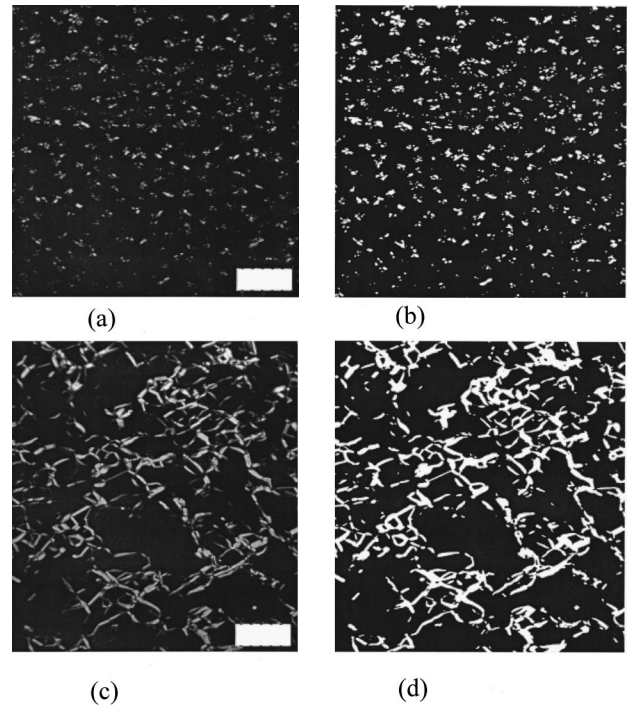


FIG. 7. (a) Gray-scale image of a sample of tallow. (b) Thresholded image of (a). (c) Gray-scale image of a sample of Salatrim®. (d) Thresholded image of (c). The horizontal length of the inset bar represents 0.005 mm.

crystal networks. Since what we are primarily interested in is how the fractal dimension affects the elastic constant, a plot of the elastic constant of the network normalized with respect to the pre-exponential term  $\gamma$  against the rheologically

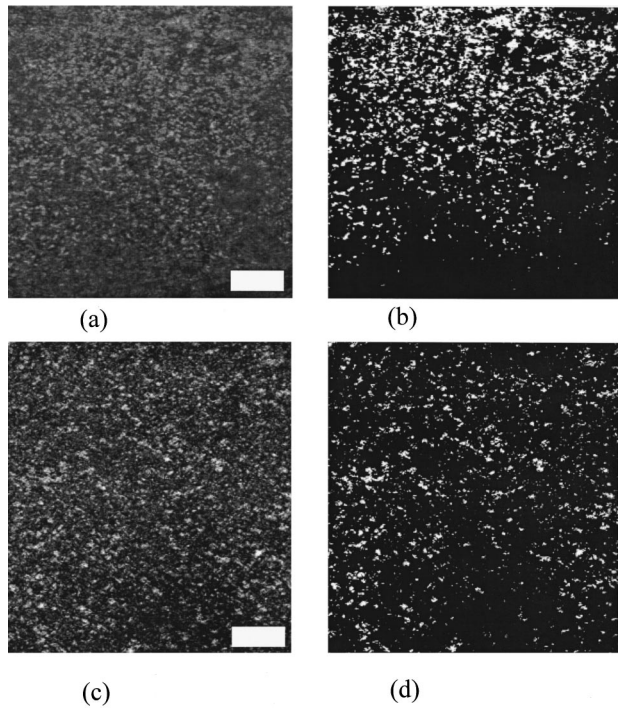


FIG. 6. (a) Gray-scale image of a sample of cocoa butter. (b) Thresholded image of (a). (c) Gray-scale image of a sample of milkfat. (d) Thresholded image of (c). The horizontal length of the inset bar represents 0.005 mm.

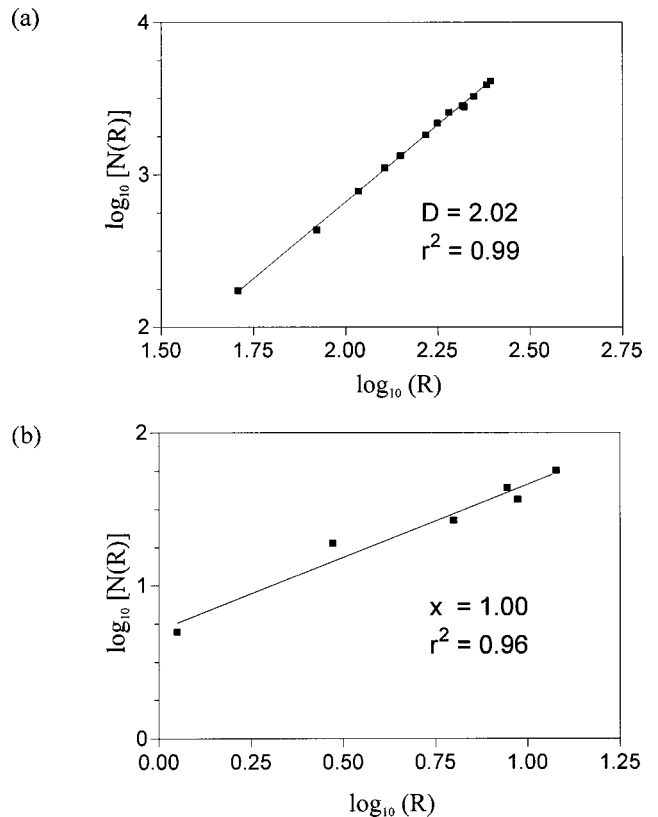


FIG. 8. Determination of  $D$  and  $x$  —  $\log_{10}(N(R))$  vs  $\log_{10}(R)$  for a sample of milkfat. The solid line is a best fit calculated by linear regression.

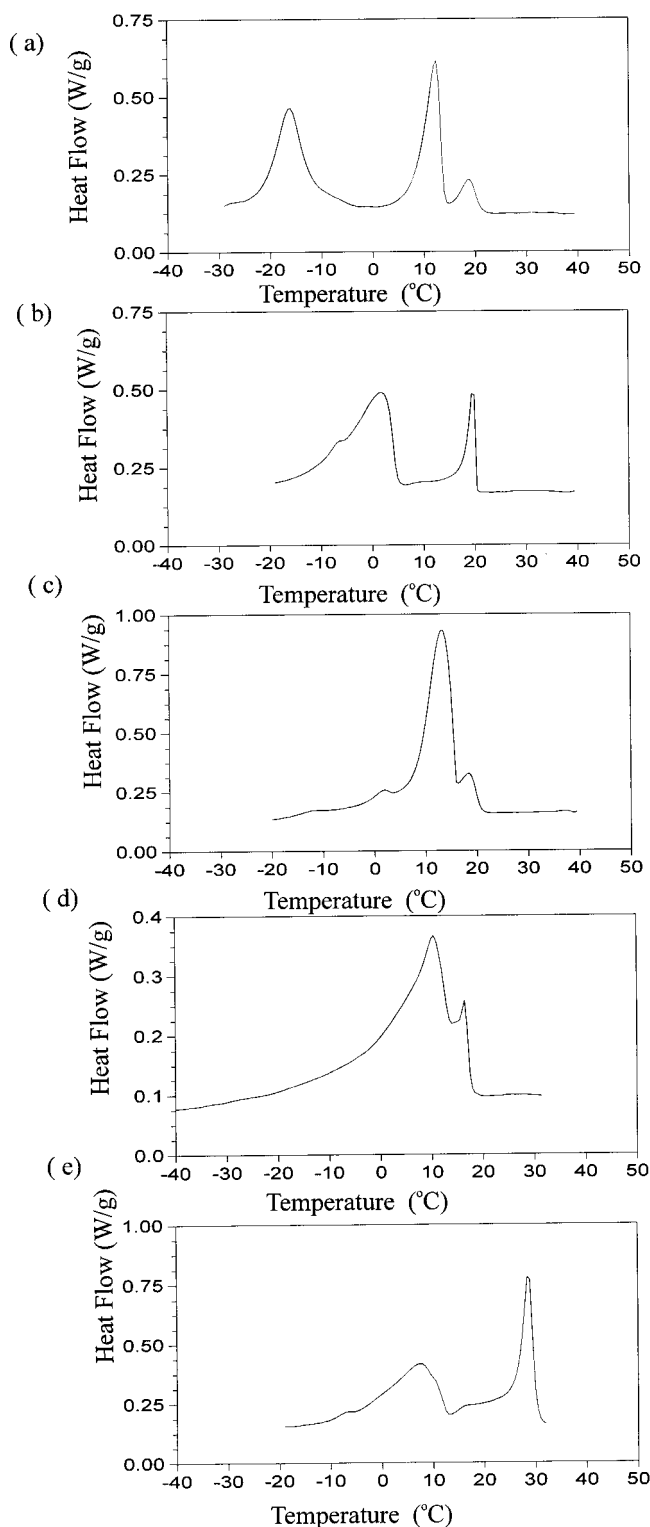


FIG. 9. Crystallization curves for samples of (a) lard, (b) palm oil, (c) cocoa butter, (d) milkfat, and (e) tallow. The area under peaks in the figure represents the energy released.

calculated fractal dimension using the weak-link theory of Shih *et al.* [30] was made, as shown in Fig. 10. The vertical error bars reflect the uncertainty in the rheologically calculated value of elastic constant and the exponent  $m$ . All of the normalized elastic constants for the various fats were calculated for a 70%  $\Phi$  value (i.e.,  $\Phi = 0.7$ ). The solid line repre-

sents the theoretical normalized elastic constant as a function of fractal dimension, and the equation of this line is

$$\frac{G'}{\gamma} = 0.7^{1/(3-D)} \quad (12)$$

## V. DISCUSSION

A direct proportionality relationship exists between the shear elastic modulus of fat crystal networks and the hardness index of the network, as is demonstrated in Fig. 4(a). Therefore, this establishes the storage or elastic modulus  $G'$  as a good indicator of the macroscopic consistency of fat crystal networks, and justifies our use of it as such.

As shown by Fig. 10, the theoretical curve of Eq. (12) predicts that the normalized elastic constant should decrease with increasing fractal dimension. The standard error bars represent the extent to which the fat systems studied rheologically deviate from this trend. As shown by Fig. 10, taking the error bars into consideration, the general trend of the theoretical curve is closely followed. A one way analysis of variance performed on this plot using GRAPHPAD (San Diego, CA) suggests that the normalized elastic constant strongly depends on the fractal dimension ( $P < 0.0001$ ). The ramifications of this plot are important. It suggests that if one can influence the fractal dimension of a particular fat by processing conditions, one can manufacture model fats, i.e., alter processing conditions to make softer or harder fats, using fractal dimension as an indicator of level of hardness. One must realize here that this presupposes that the pre-exponential term  $\gamma$  remains constant. We believe that this term is a function of the lipid composition and the crystal habit present in the network. However, it is conceivable that one can constrain the polymorphic nature of the network to remain constant while one manipulates processing conditions to affect changes in fractal dimension. The fact that under these circumstances the measured fractal dimension acts as an indicator of hardness is invaluable to the food chemist or food engineer, whose job it is to develop fat crystal networks with specific hardness index requirements. Before this work, no such indicator existed. One can argue that the process of measuring the fractal dimension via rheological analysis negates the need to use the fractal dimension as an indicator, since one is in fact measuring elastic constants directly. This is true, but the real power of this analysis lies in the fact that image analysis of pictures of the microstructure of the fat crystal networks provide highly accurate measurements of fractal dimension, as shown in Table II. This means that one can perform product development without the need to purchase highly expensive and specialized equipment such as the CarriMed rheometer or a DMA. Additionally, this opens the door to analysis of the elastic properties of softer fat crystal networks, since these are unsuitable for analysis by the rheological means currently available. The operation of rheometers of the type used in this study is also highly specialized, and requires some amount of skill. Fractal dimensions calculated from image analysis of the fat crystal network can be automated by the use of an easily written software program for an ordinary IBM personal computer. Additionally, most laboratories possess a PLM and some means to capture images from it. For the food chemist or

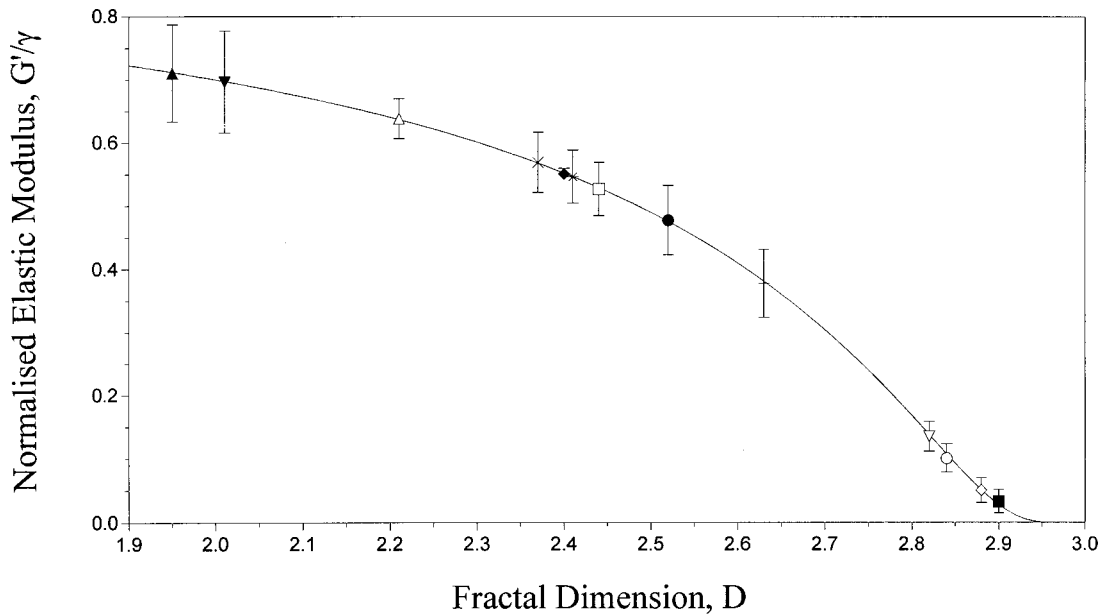


FIG. 10.  $G'/\gamma$  as a function of  $D$ . The solid line represents Eq. (12), symbols with error bars represent average values of rheological measurements and their standard errors.  $\blacktriangle$ , milkfat DMA 3.  $\blacktriangledown$ , milkfat DMA 4.  $\triangle$ , CIE milkfat 2.  $\times$ , cocoa butter 1.  $\blacklozenge$ , cocoa butter DMA 2.  $*$ , tallow.  $\square$ , NIE milkfat 2.  $\bullet$ , EIE milkfat 1.  $+$ , NIE milkfat 1.  $\nabla$ , NIE palm oil.  $\circ$ , CIE lard.  $\diamond$ , NIE lard.  $\blacksquare$ , Salatrim™.

food engineer, therefore, calculation of fractal dimensions from images of the network would provide a fast and easily performed method of determining the relative hardness of experimental products. Additionally, it is conceivable that the fractal dimension can be incorporated into quality control considerations of products that have already been designed. Because of the ease of calculation, regular checks of the fractal dimension of a particular fat crystal network being manufactured would provide a good indication if the fat is maintaining its consistency requirements.

It is an interesting fact that the fractal dimensions reported in Table II that were calculated from an image analysis of the microstructure of the fat networks, represent averages of fractal dimensions calculated from samples of different values of  $\Phi$  of the same fat. This is interesting because it suggests that the spatial distribution of the fat network remains the same, regardless of the amount of solid within the network. This supports the theory that the fractal dimension is a function of the heat and mass transfer characteristics of the network. It also nominates the fractal dimension of a fat crystal network as a fundamental constant of that network, and therefore underlines the difference of fat network structure from crystal structure, which is characterized by lattice constants.

At this point, Salatrim™ must be singled out as an example of a system that defied our calculation of a fractal dimension via image analysis. The reason for this is that there was no clear indication of microstructural elements within our image. The structure of Salatrim™ is very interesting and may warrant further investigation, but it is very different from the structure of a natural fat system, Salatrim™ being a synthetic randomly structured fat. Because of this, we have not calculated a fractal dimension for Salatrim™ via image analysis. It is included here purely for interest, and as an example of a system for which our determination of fractal dimension via image analysis failed.

However, it is conceivable that this network may be analyzed using our methods if the image of the network was of a higher resolution.

The parameters influencing the fractal dimension of a network may be inferred from an observation of the images representing the microstructural elements of the network and the corresponding DSC plot of heat flow as a function of temperature. From the images (Figs. 5–7), it can be seen that milkfat and cocoa butter represent the most disordered, amorphous structures. The order in the packing of the microstructural elements and the definition of the microstructural elements themselves increases in going from tallow to lard to palm oil. The fractal dimension of the systems increases in the order, milkfat, cocoa butter, tallow, palm oil, and lard. The seeming discrepancy in the order of the palm oil and lard systems could be due to the fact that these two systems have fractal dimensions that are very close to each other: 2.82 for palm and 2.86 for lard. From this qualitative observation, it seems that the fractal dimension increases for systems with increasingly defined microstructural elements, which pack in an increasingly ordered manner. This would seem to indicate then that those systems with a sharp nucleation step, i.e., those systems that undergo most of their nucleation in a narrow temperature range as the sample crystallizes from the melt, will have higher fractal dimensions. Samples with instantaneous nucleation characteristics will have nucleation sites that are more ordered due to heat transfer considerations. This is so because the heat released from the nucleation events would have to be dissipated throughout the network, and the most effective way of heat transfer would be an ordered array of sites. The subsequent growth of the network via a mass- and heat-transfer-limited process will also influence the fractal dimension. If the nucleation sites serve as templates for the growth of microstructural elements, there seems to be more order, whereas if the growth of the network is not restricted to the nucleation cen-

ters, the structure becomes more amorphous. The mass- and heat-transfer effects are of course governed by the processing conditions, i.e., temperature history, of the crystallization procedure, and, therefore, fractal dimension is strongly influenced by processing conditions.

The various fractions within the particular fat crystal network and the temperatures at which and the size of the temperature range over which they crystallize will therefore fundamentally affect the fractal dimension. Referring to the DSC curve shown in Fig. 9(a), lard has a fraction that crystallizes at 20 °C and one in the vicinity of 12 °C. Since our lard samples were crystallized at 5 °C, the fraction at -15 °C would not have been present in our sample. Both the peaks at 20 and 12 °C are sharp in that the full width at half maximum (FWHM) values are very small, the smaller peak at 20 °C most probably setting the nucleation template for the formation of the microstructural elements. The crystallization curve for palm oil, shown in Fig. 9(b), shows an extremely sharp peak at 20 °C, with an even smaller FWHM than demonstrated by the lard peaks, which sets the nucleation template. The peak however trails off from 20 to 5 °C, thereby probably leading to some gradual crystallization which may have contributed to some disorder in the packing of the microstructural elements. The peak below 5 °C is not considered in our analysis, because that fraction would not have crystallized in our sample, since it was held at 5 °C. However, the lard and palm oil curves both indicate the formation of very ordered systems, which is supported by the images of the microstructural network of these systems, shown in Fig. 5, and by extremely high fractal dimensions. The crystallization curve for cocoa butter shown in Fig. 9(c) has a peak in the vicinity of 10 °C that has a higher FWHM than the peaks in palm oil and lard, and this peak also trails off gradually, leading to more disorder in the system. The subsequent decrease in fractal dimension is also noted. Figure 9(d) shows a DSC curve for milkfat, with a peak at approximately 10 °C. This peak has a larger FWHM than the peak in cocoa butter, and trails off indefinitely, leading to no clearly defined nucleation template. Crystallization occurs continuously, and this will lead to a more amorphous system, which is supported by the image of milkfat shown in Fig. 6(c). The DSC curve for tallow, shown in Fig. 9(e), has an extremely sharp peak in the vicinity of 28 °C, with a FWHM value approximately the same as the peak at 20 °C in the DSC curve of palm oil. However, there is another very broad peak in the vicinity of 10 °C which would have contributed crystallization species to the formation of the microstructural network. The presence of this peak would almost certainly have destroyed the order of the nucleation template set by the fraction that crystallizes in the vicinity of 20 °C. This is supported by the image of tallow shown in Fig. 7(a), for although it is much more ordered than both milkfat and cocoa butter, it is much less ordered than both palm and lard. The value of the fractal dimension for tallow also reflects this order: 2.42, as opposed to 2.31 for cocoa butter and 2.82 for palm oil.

Having outlined how the presence of different fractions and the temperature ranges over which they crystallize affect the fractal dimension, it is important to discuss how we can exploit knowledge of the different fractions within a fat to alter the fractal dimension and therefore elastic properties. By increasing the rate of cooling of the particular fat being

crystallized from the melt, one can render the peaks of any particular fraction sharper, thereby introducing more order. Additionally, one can constrain the temperature at which the fat is crystallized, thereby eliminating entirely unwanted fractions that may introduce disorder. Alternatively, the converse is also true, where one can slow the rate of cooling if a smaller fractal dimension, and therefore a harder fat, is required.

While the value of the fractal dimension of the fat network as an indicator of hardness cannot be denied, it must be understood that the value of the pre-exponential term  $\gamma$  is also equally as important. For example, from Table I, although the fractal dimensions of NIE lard and palm oil are very close, the corresponding values of  $\gamma$  are five orders of magnitude different. This means that these fats would have widely different hardness indices, which they do. Therefore, it is also of utmost importance to characterize factors that influence  $\gamma$ , and work in our laboratory is underway to study the factors influencing this term.

Finally, it should be pointed out that we have only considered the weak link regime of Shih *et al.* One of the main reasons for this is due to some early work published by Heertje and co-workers [6,7] where it was shown that, under stress, the microstructures present in a fat crystal network are separated by a greater distance than in the unstressed state, but the nature of the microstructures themselves remains intact. This seems to indicate that the links between microstructures are stressed rather than the links between the microstructural elements composing each microstructure. Additionally, our measurements of fractal dimensions from our images agree extremely well with fractal dimensions calculated using rheological data and assuming the weak-link regime. Fractal dimensions calculated using the strong-link regime assumption do not agree with fractal dimensions measured from image analysis.

## VI. CONCLUSIONS

The fractal dimension of the microstructural network of a fat crystal network is an important indicator of the elastic constant of the network, and therefore an indicator of the hardness of the fat crystal network. Furthermore, the fractal dimension, as well as the fractal backbone dimension or chemical length exponent, may be accurately calculated from PLM images of the network, taken at the microstructural level of structure.

## ACKNOWLEDGMENTS

The authors thank Professor Alan J. Slavin, Rekha Narine, and Laurette McCormick for proofreading the manuscript. The help of Professor Robert Lencki is also acknowledged for his discussions of the theory. Dr. M. L. Herrera and Professor Richard Hartel are acknowledged for their help with the DMA analysis and Stephan Jampen for help with the CarriMed analysis. The financial support of the Natural Sciences and Engineering Research Council of Canada (NSERC) is gratefully acknowledged.

- [1] A. J. Haighton, *J. Am. Oil Chem. Soc.* **36**, 345 (1959).
- [2] M. Hayakawa and J. M. de Man, *J. Texture Stud.* **13**, 201 (1982).
- [3] J. Lefebvre, *J. Am. Oil Chem. Soc.* **60**, 247 (1983).
- [4] D. Rousseau, A. R. Hill, and A. G. Marangoni, *Food Res. Int.* (to be published).
- [5] I. Heertje, M. Leunis, W. J. M. van Zeyl, and E. Berends, *Food Microstruct.* **6**, 1 (1987).
- [6] A. C. Juriaanse and I. Heertje, *Food Microstruct.* **7**, 181 (1988).
- [7] I. Heertje, *Food Struct.* **12**, 77 (1993).
- [8] M. van den Tempel, *J. Colloid Sci.* **16**, 284 (1961).
- [9] J. M. de Man and A. M. Beers, *J. Texture Stud.* **18**, 303 (1987).
- [10] C. J. Nederveen, *J. Colloid Sci.* **18**, 1418 (1963).
- [11] J. M. P. Papenhuijzen, *Rheol. Acta* **10**, 493 (1971).
- [12] J. M. P. Papenhuijzen, *Rheol. Acta* **11**, 73 (1972).
- [13] R. Vreeker, L. L. Hoekstra, D. C. den Boer, and W. G. M. Agteroff, *Colloids Surface* **65**, 185 (1992).
- [14] S. F. Edwards and R. B. S. Oakeshott, *Physica D* **38**, 88 (1989).
- [15] M. van den Tempel, *J. Colloid Interface Sci.* **71**, 18 (1979).
- [16] H. Kamphuis, R. J. J. Jongschaap, and P. F. Mijneiff, *Rheol. Acta* **23**, 329 (1984).
- [17] H. Kamphuis and R. J. J. Jongschaap, *Colloid Polym. Sci.* **263**, 1008 (1985).
- [18] B. B. Mandelbrot, *The Fractal Geometry of Nature* (Freeman, New York, 1982).
- [19] P. G. de Gennes, *Scaling Concepts in Polymer Physics* (Cornell University Press, Ithaca, NY, 1979).
- [20] Mats Standing, Maud Langton, and Anne-Marie Hermansson, *Food Hydrocolloids* **7**, 195 (1993).
- [21] R. Vreeker, L. L. Hoekstra, D. C. den Boer, and W. G. M. Agterof, *Food Hydrocolloids* **6**, 423 (1992).
- [22] Leon G. B. Bremer, Ton van Vliet, and Pieter Walstra, *J. Chem. Soc., Faraday Trans.* **85**, 3359 (1989).
- [23] D. A. Weitz and M. Oliveria, *Phys. Rev. Lett.* **52**, 1433 (1983).
- [24] W. D. Brown and R. C. Ball, *J. Phys. A* **18**, L517 (1985).
- [25] M. Matshushita, K. Mumida, and Y. Sawada, *J. Phys. Soc. Jpn.* **54**, 2786 (1985).
- [26] W. D. Brown, Ph.D. dissertation, University of Cambridge, 1987.
- [27] R. C. Sonntag and W. B. Russel, *J. Colloid Interface Sci.* **116**, 485 (1987).
- [28] R. Buscall, P. D. A. Mills, J. W. Goodwin, and D. W. Lawson, *J. Chem. Soc., Faraday Trans.* **84**, 4249 (1988).
- [29] R. C. Ball, *Physica D* **38**, 13 (1989).
- [30] W. H. Shih, W. Y. Shih, S. I. Kim, J. Lin, and I. A. Aksay, *Phys. Rev. A* **42**, 4772 (1990).
- [31] N. B. Uriev and I. Ya. Ladyzhinsky, *Colloids Surf., A* **108**, 1 (1996).
- [32] A. G. Marangoni and D. Rousseau, *J. Am. Oil Chem. Soc.* **73**, 991 (1996).
- [33] D. Rousseau, K. Forestiere, A. R. Hill, and A. G. Marangoni, *J. Am. Oil Chem. Soc.* **73**, 963 (1996).
- [34] D. Rousseau, A. R. Hill, and A. G. Marangoni, *J. Am. Oil Chem. Soc.* **73**, 973 (1996).
- [35] D. Rousseau, A. R. Hill, and A. G. Marangoni, *J. Am. Oil Chem. Soc.* **73**, 983 (1996).
- [36] D. Rousseau and A. G. Marangoni, *J. Agric. Food Chem.* **46**, 2368 (1998).
- [37] D. Rousseau and A. G. Marangoni, *J. Agric. Food Chem.* **46**, 2375 (1998).
- [38] D. Rousseau, K. R. Jeffrey, and A. G. Marangoni, *J. Am. Oil Chem. Soc.* **75**, 1833 (1998).
- [39] A. G. Marangoni and D. Rousseau, *J. Am. Oil Chem. Soc.* **75**, 1265 (1998).
- [40] A. G. Marangoni and D. Rousseau, *J. Am. Oil Chem. Soc.* **75**, 1633 (1998).
- [41] S. S. Narine and A. G. Marangoni, *J. Am. Oil Chem. Soc.* **76**, 7 (1999).
- [42] R. Jullien and R. Botet, *Aggregation and Fractal Aggregates* (World Scientific, Singapore, 1987).
- [43] P. Meakin, *Adv. Colloid Interface Sci.* **28**, 249 (1988).
- [44] G. Dietler, C. Aubert, D. S. Cannel, and P. Wiltzinus, *Phys. Rev. Lett.* **57**, 3117 (1986).
- [45] M. Kellens, W. Meeussen, and H. Reynaers, *J. Am. Oil Chem. Soc.* **69**, 906 (1992).
- [46] P. Meakin, *Phys. Rev. Lett.* **51**, 1119 (1983).
- [47] M. Kolb, R. Botet, and R. Jullien, *Phys. Rev. Lett.* **51**, 1123 (1983).
- [48] M. Kolb and R. Jullien, *J. Phys. (France) Lett.* **45**, 977 (1984).
- [49] W. Mohr and J. Wellm, *Milchwissenschaft* **3**, 234 (1948).
- [50] P. A. Rebinder and N. A. Semenenko, *Dokl. Akad. Nauk SSSR* **64**, 835 (1949).
- [51] N. N. Agranat and M. P. Volarovich, *Kolloidn. Zh.* **19**, 3 (1957).
- [52] C. W. Hoerr, *J. Am. Oil Chem. Soc.* **37**, 539 (1960).
- [53] C. E. Keen, S. J. A. Buk, and D. A. Levison, *J. Clinical Pathology*, **47**, 1028 (1994).
- [54] J. R. Parker, *Practical Computer Vision Using C* (Wiley, New York, 1994), pp. 126–145.
- [55] Kenneth Falconer, *Fractal Geometry* (Wiley, Chichester, 1990).
- [56] Richard M. Crownover, *Introduction to Fractals and Chaos* (Jones and Bartlett, Boston, 1995).
- [57] Philip M. Iannaccone and Mustafa K. Khokha, in *Fractal Geometry in Biological Systems*, edited by Philip M. Iannaccone and Mustafa K. Khokha (CRC Press, Boca Raton, FL, 1996), pp. 3–11.
- [58] Gabriel Landini, in *Fractal Geometry in Biological Systems* (Ref. [57]), pp. 226–242.